Title: Biosynthetic intermediates of the enterobacterial common antigen overcome outer membrane lipid dyshomeostasis in *Escherichia coli*

Authors: Xiang'Er Jiang[a#], Rahul Shrivastava[a#], Wee Boon Tan[b#], Deborah Chwee San Seow[c], Swaine Lin Chen[d,e], Xue Li Guan[c], Shu-Sin Chng[a,b*]

Affiliations:

[a]Department of Chemistry, National University of Singapore, Singapore 117543.

[b]Singapore Center for Environmental Life Sciences Engineering, National University of Singapore (SCELSE-NUS), Singapore 117456.

[c]Lee Kong Chian School of Medicine, Nanyang Technological University, Singapore 636921.

[d]Yong Loo Lin School of Medicine, National University of Singapore, Singapore 119228.

[e]Genome Institute of Singapore, Agency for Science, Technology and Research (A*STAR), Singapore 138672.

[#]These authors contributed equally to the work.

*To whom correspondence should be addressed. E-mail: chmchngs@nus.edu.sg

Keywords: Tol-Pal complex, ECA, outer membrane, lipid homeostasis, phospholipid transport, vancomycin resistance

Abstract

The outer membrane (OM) is an essential component of the Gram-negative bacterial cell envelope that protects cells against external threats such as antibiotics. To maintain a stable and functional OM barrier, cells require distinct mechanisms to ensure a balance of proteins and lipids in the membrane. Crucial to this is the proper transport and assembly of various OM components, of which the process of phospholipid (PL) transport is least understood. How OM assembly pathways are coordinated to achieve homeostasis is also unclear. In this study, we set out to identify potential mechanism(s) that can alleviate OM lipid dyshomeostasis in *Escherichia coli*. Cells lacking the Tol-Pal complex accumulate excess PLs in the OM due to defective retrograde PL transport. Here, we isolated mutations in enterobacterial common antigen (ECA) biosynthesis that restore OM barrier function in these strains; build-up of biosynthetic intermediates along the ECA pathway is key to this rescue. Interestingly, these ECA mutations re-establish OM lipid homeostasis in cells lacking the Tol-Pal complex yet do not act by restoring retrograde PL transport. Furthermore, a novel diacylglycerol pyrophosphoryl-linked ECA species structurally similar to PLs can be detected in the inner membrane of ECA mutants. We therefore propose a model where these unique species may modulate anterograde PL transport to overcome OM lipid dyshomeostasis. Our work provides insights into bacterial lipid transport across the cell envelope and highlights previously unappreciated effects of ECA intermediates in OM biology.

Author Summary

Biological membranes define cellular boundaries, allow compartmentalization, and represent a prerequisite for life; yet, our understanding of membrane biogenesis and stability remain rudimentary. In Gram-negative bacteria, the outer membrane prevents entry of toxic substances, conferring intrinsic resistance against many antibiotics. How the outer membrane is assembled, specifically lipid trafficking processes are not well understood. How this membrane is stably maintained is also unclear. In this study, we discovered that intermediates along the biosynthetic pathway of an exopolysaccharide exhibit stabilizing effects on outer membranes with lipid imbalance in *Escherichia coli*. Our work suggests that these intermediates modulate phospholipid trafficking within the double-membrane cell envelope to achieve outer membrane lipid homeostasis. Furthermore, it provides a starting point to begin identifying hitherto unknown phospholipid transport systems in Gram-negative bacteria, which are potential targets for the development of future antibiotics.

Introduction

Gram-negative bacteria are surrounded by a multilayered cell envelope consisting of the inner membrane (IM), the peptidoglycan layer, and the outer membrane (OM). This envelope structure, in particular the OM, plays an essential role in preventing toxic molecules from entering the cell, contributing to intrinsic resistance of Gram-negative bacteria against many antibiotics and detergents [1]. The OM bilayer is asymmetric and has a unique lipid composition, comprising lipopolysaccharides (LPS) in the outer leaflet and phospholipids (PLs) in the inner leaflet. In the presence of divalent cations, LPS molecules in the outer leaflet pack together to form an impervious monolayer [2]; OM structure and lipid asymmetry are thus key determinants for its barrier function. Furthermore, the OM is essential for growth, highlighting the importance of understanding how it is established and maintained.

The biogenesis of the OM has been relatively well studied. Key components, including LPS, integral β-barrel proteins, and lipoproteins, are transported and assembled unidirectionally into the OM by the Lpt [3], Bam [4], and Lol machinery [5], respectively. Trafficking of bulk PLs between the IM and the OM is less well characterized, although it is known to proceed in both directions [6-8]. To build a stable and functional OM, the synthesis, transport, and assembly of these different components need to be coordinated. Regulatory cascades, including the σ^E, Cpx and Rcs signaling pathways, sense and control the levels of different OM components, especially in the context of envelope stress [9-11]. Another mode of coordination involves interdependency among the various OM assembly systems; notably, the presence of a β-barrel protein (LptD) and

a lipoprotein (LptE) in the OM LPS translocon implies that LPS transport requires functional Bam and Lol pathways. A third mechanism, which is related to OM homeostasis, suggests that the cell maintains a high flux of PLs to the OM to offset problems created by changes in levels of other OM components [12]. Here, excess PLs can be transported back to the IM in a manner dependent on the Tol-Pal complex.

The Tol-Pal complex is a conserved multi-protein system that forms an energy dependent trans-envelope bridge across the cell envelope in Gram-negative bacteria [13-15]. It comprises two sub-complexes: TolQRA in the IM and TolB-Pal at the OM. The function of the Tol-Pal complex has been elusive, although it is known to be generally important for OM stability and integrity [13]. Recently, we demonstrated that the Tol-Pal complex is involved in the maintenance of OM lipid homeostasis in *Escherichia coli* [12]. Cells lacking the intact complex accumulate excess PLs in the OM due to defects in retrograde (OM-to-IM) PL transport. This increase in PL content in the OM contributes to many known phenotypes in *tol-pal* mutants, including hypersensitivity to antibiotics and detergents, leakage of periplasmic content, and OM hypervesiculation [13, 16]. The Tol-Pal complex is also involved in OM invagination during cell division [17]. Overall, it is believed that the Tol-Pal complex mediates retrograde transport of bulk PLs to maintain homeostasis and stability at the OM.

OM biogenesis and maintenance are complex processes, so there are likely other mechanisms involved in controlling the levels of OM components. To gain more insight into OM homeostasis, we asked whether cells lacking the Tol-Pal complex could restore their OM barrier function by compensatory mutations in other pathways. We found that disruption in the

biosynthesis of enterobacterial common antigen (ECA), a cell surface polysaccharide in the Enterobacteriaceae family [18], rescues OM permeability defects in *tol-pal* mutants. The accumulation of ECA intermediates is responsible for this rescue. Interestingly, we demonstrate that OM lipid homeostasis is restored even though retrograde PL transport is still defective. Our work suggests a model where cells overcome the problem of excess PL accumulation in the OM by inhibiting anterograde PL transport.

Results

Loss-of-function mutations in ECA biosynthesis rescue OM permeability defects in *tol-pal* mutants

Cells lacking the Tol-Pal complex have compromised OM integrity due to the accumulation of excess PLs [12]. To identify other pathways important for maintaining OM lipid homeostasis, we sought to isolate genetic suppressor mutations that could restore OM barrier function in a Δ*tol-pal* mutant. We selected for suppressors that rescue sensitivity to vancomycin, the large cell wall-targeting antibiotic that cannot penetrate an intact and functional OM [19]. Cells have no intrinsic mechanism to alter cell wall structure to give rise to resistance against vancomycin; consistently, suppressor colonies appeared at a low frequency of ~1 x 10^{-9}. We obtained 36 individual suppressor strains, all of which exhibited stable resistance phenotypes against vancomycin similar to a wild-type (WT) strain. We further examined the susceptibilities of these

strains against other commonly used antibiotics, including rifampicin and erythromycin. An intact OM also impedes the entry of rifampicin and erythromycin but less effectively than against vancomycin [19]. Based on the observed phenotypes, these suppressors can be broadly categorized into four classes. Class I suppressors exhibit near wild-type level resistance against all antibiotics tested (S1A Fig). Class II and III suppressors are fully resistant to vancomycin and one other antibiotic, while Class IV strains are only resistant to vancomycin. Class I suppressor strains appear to have restored OM barrier function. Consistent with this, many of these strains do not leak, or release less, periplasmic RNase I into the media during growth when compared to the parent Δ*tol-pal* mutant (S1B Fig). We sequenced the genomes of the parent strain and all eight Class I suppressors. Each suppressor strain contains multiple mutations relative to the parent Δ*tol-pal* mutant (S1 Table); interestingly, all of these strains have mutations in genes involved in the biosynthesis of ECA (*wecB*, *wecC*, or *wecF*).

Six strains contain mutations in *wecC*, which encodes a dehydrogenase enzyme in the ECA synthesis pathway [18, 20]. A 6-bp in-frame insertion in *wecC*, termed *wecC**, is common to four of these strains, suggesting that this allele may be important for restoring OM barrier function in the Δ*tol-pal* mutant. To validate this, we re-constructed the *wecC** mutation in the native locus using a negative selection technique [21], and confirmed that this allele alone is able to rescue vancomycin sensitivity (Fig 1A) and periplasmic leakiness in Δ*tolQ*, Δ*tolA*, and Δ*tolB* strains (S2A Fig). The effects of *wecC** on these phenotypes are only partial, however, suggesting that other mutations found in the original suppressor strains may also contribute to restoring OM function. Supporting this idea, the *wecC** mutation does not restore resistance of the *tol-pal*

141 strains against erythromycin and rifampicin (S2B Fig). Rifampicin (MW ~823) and erythromycin
142 (MW ~734) are much smaller than vancomycin (MW ~1449). It appears that the *wecC** mutation
143 only restores OM barrier function in the *tol-pal* mutant against the passage of larger molecules,
144 including vancomycin and periplasmic proteins (e.g. RNase I).

145 The *wecC** mutation results in the insertion of two amino acids (Pro and Gly) five residues
146 away from the predicted active site Cys in the full-length protein, suggesting that WecC function
147 may be disrupted. Consistent with this, we did not detect any ECA in strains containing this
148 *wecC** allele (Fig 1C). Furthermore, we showed that deletion of *wecC* also partially restores
149 vancomycin resistance in *tol-pal* strains (Fig 1B and C). We isolated *wecB* and *wecF* mutations
150 in two of the Class I suppressor strains (Table S1); we therefore constructed Δ*wecB* and Δ*wecF*
151 mutants to test their rescue phenotypes. Both null mutations partially rescue vancomycin
152 sensitivity in the Δ*tolA* strain (Fig 1D). We conclude that loss-of-function mutations in ECA
153 biosynthesis restore the function of the OM in strains lacking the Tol-Pal complex.

154

155 **Suppression of OM permeability defects in *tol-pal* strains by mutations in ECA biosynthesis**
156 **is independent of Rcs phosphorelay pathway and/or capsular polysaccharide biosynthesis**

157

158 Mutations in the ECA pathway are known to trigger the Rcs phosphorelay stress response [22].
159 *tol-pal* mutations also strongly activate the Rcs signaling cascade [23]. Consequently, combined
160 *tol-pal*/ECA mutant colonies exhibit strongly mucoid phenotypes, presumably due to the
161 over-production of capsular polysaccharides (colanic acids), which is regulated by the Rcs

pathway [24, 25]. We therefore considered whether hyperactivation of the Rcs stress response or up-regulation of colanic acid biosynthesis contributed to the suppression of vancomycin sensitivity by ECA mutations in the *tol-pal* strains. To test this idea, we examined vancomycin sensitivity in *rcsC* (encoding the histidine sensor kinase of the Rcs pathway) [24] or *wcaJ* (encoding the glycosyl transferase that initiates colanic acid biosynthesis) [26] mutants. Deleting *rcsC* or *wcaJ* did not prevent the Δ*wecC* mutation from suppressing vancomycin sensitivity in the Δ*tolA* strain; instead, the Δ*rcsC* Δ*tolA* Δ*wecC* and Δ*wcaJ* Δ*tolA* Δ*wecC* mutants display full resistance against vancomycin, similar to WT cells (Fig 2A). Furthermore, the Δ*wecC* mutation still partially rescued periplasmic leakiness in Δ*rcsC* and Δ*wcaJ* background strains (Fig 2B). The mechanism by which the Δ*wecC* mutation suppresses *tol-pal* phenotypes is therefore independent of the Rcs phosphorelay.

We have observed that the Δ*wecC* mutation rescues vancomycin sensitivity in the Δ*tolA* strain; however, we noted that different transductants display varying extents of suppression (S3 Fig). We found that removing RcsC or WcaJ greatly improved the consistency of suppression of the Δ*tolA* phenotype by the Δ*wecC* mutation. This suggests that the initial variability in suppression could be due to varying mucoidal phenotypes. To eliminate this inconsistency, we used strains deleted of *wcaJ* for the rest of this study.

Accumulation of ECA intermediates along the biosynthetic pathway is necessary for rescue of *tol-pal* phenotypes

The initial steps of ECA biosynthesis involve successive addition of three sugar moieties (*N*-acetyl-D-glucosamine (GlcNAc), *N*-acetyl-D-mannosaminuronic acid (ManNAcA), and 4-acetamido-4,6-dideoxy-D-galactose (Fuc4NAc)) to the undecaprenyl phosphate (und-P) lipid carrier to form Lipid III^{ECA} [18, 27]. After its synthesis at the inner leaflet of the IM, Lipid III^{ECA} is flipped across the membrane by WzxE [28]. This trisaccharide repeating unit is then polymerized by WzyE to form the complete ECA polymer, whose polysaccharide chain length is regulated by WzzE [29, 30]. The whole ECA polymer, which is now carried on undecaprenyl pyrophosphate (und-PP), is finally transferred to form a phosphatidyl-linked species (ECA_{PG}) before being transported to the OM [31-33] (Fig 3A). The enzymes mediating the last two steps are not known. Of note, a small amount of ECA polymer may be found attached to LPS (ECA_{LPS}) or exists in a soluble cyclic form (ECA_{CYC}) in the periplasm [18].

We have shown that loss-of-function mutations in *wecB*, *wecC*, and *wecF* rescue vancomycin sensitivity in *tol-pal* mutants (Fig 1). These mutations result in both loss of ECA itself and the build-up of Lipid I^{ECA} or Lipid II^{ECA} intermediates along the biosynthetic pathway (Fig 3A). To test whether ECA loss is important, we mutated *wecA*, which encodes the enzyme that catalyzes the first committed step in ECA biosynthesis [34]. Interestingly, we found that the Δ*tolA* Δ*wecA* mutant (in the Δ*wcaJ* background) is equally sensitive to vancomycin as the Δ*tolA* mutant (Fig 3B), suggesting that accumulation of intermediates along the ECA pathway, but not loss of ECA, is responsible for the suppression. Consistent with this idea, removing other ECA biosynthetic enzymes that result in accumulation of intermediates (Lipid I^{ECA} in Δ*wecG*, or Lipid II^{ECA} in Δ*wecE*) fully rescues vancomycin sensitivity in the Δ*tolA* mutant (Fig 3B). Importantly,

rescue of vancomycin sensitivity in these strains is completely abolished when *wecA* is also deleted (Fig 3C). We conclude that the build-up of Lipid I^{ECA} or Lipid II^{ECA} intermediates can somehow restore OM barrier function in the absence of the Tol-Pal complex.

We next tried to test whether mutations in later steps of ECA biosynthesis also suppress *tol-pal* phenotypes. However, it has been reported that blocking translocation across the IM or subsequent polymerization of Lipid III^{ECA} causes toxicity in cells. Removing WzxE, together with WzxB, the O-antigen flippase that can also transport Lipid III^{ECA}, is lethal [28] (S4A Fig). WzyE is also essential for growth [29, 35] (S4B Fig), precluding further analysis. We therefore turned our attention to WzzE. Remarkably, deletion of *wzzE* partially rescues vancomycin sensitivity in the Δ*tolA* mutant, and this phenotype is dependent on the presence of WecA (Fig 4A). Cells lacking WzzE are known to lose modality in the ECA polymer, giving rise to a more random distribution of chain lengths [30]. We validated this observation; there are relatively higher levels of shorter chain ECA, including Lipid III^{ECA} precursors, in the Δ*wzzE* mutant (Fig 4B). Taken together, our results suggest that build-up of Lipid III^{ECA} intermediates can also rescue OM defects in cells lacking the Tol-Pal complex.

Recently, it has been reported that the build-up of ECA "dead-end" intermediates in a strain with defective undecaprenyl pyrophosphate synthase (UppS) [36] can lead to sequestration of und-P, the common precursor for many sugar polymers in the cell envelope including peptidoglycan; this gives rise to severe shape defects such as filamentation and swelling [37]. Contrary to this finding, in our strains that express wild-type UppS, we did not observe major shape defects in the Δ*wecC* mutant, whether in the WT or Δ*tolA* background (S5A Fig). However,

our double *tol-pal wec* mutants often exhibit a small colony morphology. We further showed that overexpression of UppS, which can alleviate potential und-P sequestration [37], did not reverse the suppression effect of ECA mutations on vancomycin sensitivity in the Δ*tolA* mutant (S5B Fig). These results indicate that the effect of accumulation of ECA intermediates in restoring vancomycin resistance in *tol-pal* mutants is independent of und-P sequestration.

Accumulation of ECA intermediates, specifically Lipid II^{ECA}, is also known to stimulate the σ^E and Cpx stress response pathways [38]. However, we did not observe significant induction or increased stimulation of σ^E when Lipid $I/II/III^{ECA}$ intermediates were accumulated in WT or Δ*tolA* strains, respectively (S6A Fig). Removing the Cpx pathway also did not affect vancomycin resistance in the Δ*tolA* Δ*wzzE* strain (S6B Fig). We conclude that both σ^E and Cpx stress responses are not involved in the ability of accumulated ECA intermediates to restore the OM barrier function in *tol-pal* mutants.

Diacylglycerol pyrophosphoryl-linked species also accumulate in ECA biosynthesis mutants

We have shown that accumulation of ECA intermediates rescues vancomycin sensitivity in strains lacking the Tol-Pal complex. However, und-PP-linked intermediates (Lipid $I/II/III^{ECA}$) may not be the only species accumulated in ECA biosynthesis mutants. In a *Salmonella* Typhimurium Δ*rmlA* mutant, which accumulates Lipid II^{ECA}, a novel diacylglycerol pyrophosphoryl (DAG-PP)-linked species containing the first two sugars of ECA (GlcNAc and ManNAcA) was detected at comparable levels [39]. We therefore sought to determine whether

DAG-PP-linked adducts could also be found in our *E. coli* ECA mutants. Using high resolution mass spectrometry (MS), we analyzed lipids extracted from cells lacking WecG, which is expected to accumulate Lipid I^{ECA}. We demonstrated that DAG-PP-GlcNAc species are indeed present in these cells, but not in WT (Fig 5A and 5B). Specifically, we detected peaks with m/z values corresponding to DAG-PP-GlcNAc species with various fatty acid compositions in the DAG moiety, namely 32:1 (m/z 928.4927), 34:1 (m/z 956.5243), 34:2 (m/z 954.5076), and 36:2 (m/z 982.5391); these are in fact the major DAGs found in native PLs in *E. coli* [40]. Chemical structures of the 32:1 and 34:1 species were assigned and elucidated based on fragmentation patterns in MS/MS (Fig 6). Furthermore, we showed that the same species were specifically found in the IM but not the OM of the Δ*wecG* mutant, as well as the Δ*wecC* strain (Fig 5C). It is worth noting that DAG-PP has one extra phosphate moiety and is therefore structurally distinct from phosphatidic acid (i.e. diacylglycerol monophosphate or DAG-P), the final lipid carrier of ECA. How the DAG-PP-linked species are generated is not clear, but their existence highlights the need to consider possible effects of these novel lipids in ECA biosynthesis mutants, especially in the context of rescuing *tol-pal* phenotypes.

Build up of ECA intermediates restores OM lipid homeostasis in *tol-pal* mutants but not defects in retrograde PL transport

Cells lacking the Tol-Pal complex accumulate excess PLs (relative to LPS) in the OM due to defective retrograde PL transport [12]. Since mutations in the ECA biosynthetic pathway rescue

OM defects in *tol-pal* mutants (Fig 1), we hypothesized that OM lipid homeostasis is restored in these strains. To test this idea, we examined steady state OM lipid compositions in Δ*tolA* Δ*wecC* mutant cells by measuring the distribution of [^{3}H]-glycerol-labelled PLs between the IM and the OM, and also determining the ratio of PLs to LPS (both labelled with [^{14}C]-acetate) in the OM. Consistent with our previous findings, the Δ*tolA* mutant contained more PLs in the OM than WT cells (here in the Δ*wcaJ* background). Specifically, cells lacking TolA accumulate ~1.6-fold excess PLs in the OM (relative to the IM), as judged by [^{3}H] distribution (Fig 7A). Furthermore, these cells have a ~1.5-fold higher [^{14}C]-PL/LPS ratio in the OM (Fig 7B and S7 Fig). The Δ*wecC* mutation alone did not alter PL profiles in the OM. Remarkably, however, deleting *wecC* in the Δ*tolA* strain not only re-established intermembrane PL distribution, but also returned the OM PL/LPS ratio back to wild-type (Fig 7A and 7B). Notably, the Δ*wecC* mutation had no impact on LPS levels (S8 Fig). In toto, we conclude that build-up of intermediates as a result of defective ECA biosynthesis restores OM lipid homeostasis in cells lacking the Tol-Pal complex.

Cells lacking the Tol-Pal complex produce more OMVs [16]. We have previously shown that these OMVs contain an elevated PL/LPS ratio, similar to that in the OM of these cells [12], and suggested that *tol-pal* mutants hypervesiculate because of increased PL content in the OM. Given that the Δ*wecC* mutation restores OM lipid homeostasis in the Δ*tolA* strain, we asked whether OMV production in these double mutants would be reduced to WT levels. Mutations in ECA biosynthesis are known to cause slight increases in OMV formation [41]; we confirmed that this is true for the Δ*wecC* mutant (S9 Fig). Taking this into account, we observed essentially no change in the amount of OMVs produced by the Δ*tolA* Δ*wecC* strain compared to the Δ*tolA* mutant.

Interestingly, OMVs derived from the double mutant have a PL/LPS ratio similar to that in its OM, which is essentially like WT (Fig 7B and S7 Fig). It therefore appears that lipid dyshomeostasis in the OM of *tol-pal* mutants only plays no more than a minor role in the hypervesiculation phenotype. OMV production, which mainly occurs at division sites and cell poles [16], may be due to inefficient OM invagination during cell division in the absence of the Tol-Pal complex [17].

How the accumulation of ECA intermediates restores lipid homeostasis in *tol-pal* mutants is not clear; one possible mechanism involves rescuing defects in retrograde PL transport in these strains. To test this idea, we monitored the turnover of [^{32}P]-pulse-labelled OM anionic lipids in the Δ*tolA* Δ*wecC* mutant as these lipids are transported back to the IM [12]. Using this coupled assay, which we have previously developed, we established that cells lacking both TolA and WecC exhibit similar defects in retrograde PL transport when compared to the Δ*tolA* mutant (S10 Fig). Hence, intermediates accumulated in ECA biosynthesis mutants do not act to increase transport of PLs from the OM back to the IM.

Discussion

In this study, we have employed a genetic approach to gain insights into OM homeostasis in *E. coli*. We have identified suppressor mutations that can rescue OM permeability defects in cells lacking the Tol-Pal complex, which are known to contain excess PLs in their OM [12, 42]. Mutations in ECA biosynthesis restore OM lipid homeostasis (Fig 7), thus conferring vancomycin resistance and reduced periplasmic leakiness in *tol-pal* strains (Figs 1 and 2). We have further

309 demonstrated that these rescue phenotypes are due to the accumulation of intermediate species
310 along the ECA pathway (Figs 3 and 4). We propose that these species, which are likely in the IM,
311 affect OM lipid biology by modulating PL transport across the cell envelope.

312 The role of ECA in the enterobacterial cell envelope is not known. Strains that do not make
313 ECA are more sensitive to bile salts and produce more OMVs [38, 41]. Loss of cyclic ECA has
314 also been reported to modulate OM function in strains lacking YhdP, a protein of unknown
315 function [43]. These observations suggest that ECA has roles related to the OM. However, we have
316 shown that loss of ECA itself (ECA_{PG}/ECA_{LPS}/ECA_{CYC}) does not contribute to the restoration of
317 OM barrier function in cells lacking the Tol-Pal complex; instead, the build-up of ECA
318 biosynthetic intermediates is necessary for this rescue. Interestingly, accumulation of
319 und-PP-linked intermediates (in the ECA, O-antigen, and colanic acid pathways) can lead to
320 sequestration of und-P [44], the common lipid carrier also used for peptidoglycan precursors.
321 While this can give rise to shape changes, it was not obvious in our strains (S5A Fig), which have
322 functional UppS and do not synthesize O-antigens and colanic acids. Overexpression of UppS to
323 increase the pool of available und-P also did not reverse the suppression of *tol-pal* phenotypes
324 (S5B Fig). We therefore believe that restoration of OM phenotypes by ECA intermediates in cells
325 lacking the Tol-Pal complex is independent of und-P sequestration. The rescue mechanism
326 additionally does not appear to involve the major cell envelope stress response pathways (Fig 2
327 and S6 Fig).

328 Cells lacking the Tol-Pal complex accumulate excess PLs in the OM due to defective
329 retrograde PL transport [12]. We have shown that the accumulation of ECA intermediates restores

OM lipid homeostasis in *tol-pal* mutants (Fig 7), but how these intermediates act to correct the problem of excess PLs in the OM is not clear. We posit that the most direct mechanism(s) to prevent excess PL build-up at the OM would be to modulate PL transport across the cell envelope. Retrograde PL transport was not restored in the Δ*tolA* Δ*wecC* double mutant (S10 Fig); therefore, we further hypothesize that anterograde PL transport could in fact be attenuated. While und-PP-linked intermediates are expected to be accumulated in ECA mutants, we and others have also observed the corresponding DAG-PP-linked species [39]. Specifically, we have detected DAG-PP-GlcNAc only in the IM of the Δ*wecC*/Δ*wecG* strains (Fig 5), suggesting that such species are not transported to the OM. Intriguingly, the novel DAG-PP-linked species are structurally similar to PLs, which have polar headgroups linked to DAG-P (i.e. phosphatidic acid) (Fig 3A). Therefore, they could serve as substrate mimics of the yet-to-be-identified anterograde PL transport machinery, thereby inhibiting the process at the IM. Studies are underway to test this hypothesis.

How DAG-PP-linked species are made is unclear. In the canonical ECA pathway, the final polymer on the und-PP carrier is transferred via an unknown mechanism to give ECA_{PG}, a DAG-P-linked polymer, at the outer leaflet of the IM [18]. It is therefore conceivable that DAG-PP-linked species are also derived from und-PP-linked ECA intermediates in a similar fashion. That the flippase WzxE has been shown to transport an analog of Lipid I^{ECA} across the IM [28] suggests the possibility that early ECA biosynthetic intermediates can reach the outer leaflet of the IM, and somehow be converted to DAG-PP-linked species. The resulting location of these species would make sense in the proposed context of interaction with, and inhibition of, an

anterograde PL transport pathway, which presumably accepts substrates from the outer leaflet of the IM. This model is also consistent with the observation that removing WzzE, which causes accumulation of short chain ECA intermediates in the outer leaflet of the IM, similarly rescues OM phenotypes in *tol-pal* mutant strains (Fig 4A).

It is quite remarkable that our approach led to the identification of genetic interactions between the ECA pathway and OM lipid transport in *E. coli*. After they are synthesized, ECA_{PG} are transported to the OM. The mechanism for this process is not clear, but may require a system that is similar to, if not the same as, any pathway(s) for anterograde PL transport. If this were the case, the idea that DAG-PP-linked species could interfere with PL transport seems reasonable. Further investigation into the final stages of ECA assembly and transport will be required to elucidate interactions between these pathways and eventually provide new insights into lipid trafficking across the cell envelope.

Materials and methods

Strains and growth conditions. All the strains used in this study are listed in S2 Table. *Escherichia coli* strain MC4100 [*F⁻ araD139 Δ(argF-lac) U169 rpsL150 relA1 flbB5301 ptsF25 deoC1 ptsF25 thi*] [45] was used as the wild-type (WT) strain for most of the experiments. NR754, an *araD*$^{+}$ revertant of MC4100 [46], was used as the WT strain for experiments involving depletion of *wzxE* or *wzyE* from the arabinose-inducible promoter (P_{BAD}). Gene deletion mutants were constructed using recombineering [47] or obtained from the Keio collection [35]. Whenever needed, the antibiotic resistance cassettes were flipped out as described [47]. Gene deletion cassettes were transduced into relevant genetic background strains via P1 transduction [48]. The unmarked and chromosomal *wecC** allele was constructed using a negative selection technique [21]. Luria-Bertani (LB) broth (1% tryptone and 0.5% yeast extract, supplemented with 1% NaCl) and agar were prepared as previously described [48]. When appropriate, kanamycin (kan; 25 μg ml^{-1}), chloramphenicol (cm; 30 μg ml^{-1}), ampicillin (amp; 200 μg ml^{-1}) and spectinomycin (spec; 50 μg ml^{-1}) were added.

Plasmid construction. Plasmids used in this study are listed in S3 Table. Desired genes were amplified from MC4100 chromosomal DNA using the indicated primers (sequences in S4 Table). Amplified products were digested with indicated restriction enzymes (New England Biolabs), which were also used to digest the carrying vector. After ligation, recombinant plasmids were transformed into competent NovaBlue (Novagen) cells and selected on LB plates

386 containing appropriate antibiotics. DNA sequencing (Axil Scientific, Singapore) was used to
387 verify the sequence of the cloned gene.
388
389 **Generation of suppressor mutations and genome sequencing.** To isolate spontaneous
390 suppressor mutants, 10^9 BW25113 Δ*tol-pal*$^{\#}$ cells were plated on LB agar plate supplemented
391 with vancomycin (250 μg/ml) and incubated at 37ºC for 48 h. Individual colonies were picked
392 and restreaked on similar plates to verify their vancomycin resistance properties. 36 separate
393 strains were isolated and classified into four classes based on their antibiotic susceptibilities (see
394 text). To identify the genetic location of mutations in Class I suppressor mutant strains, whole
395 genome sequencing was performed. Purified genomic DNA was sheared to approximately 300
396 bp using a focused ultrasonicator (Covaris). A sequencing library was prepared using the TruSeq
397 DNA PCR Free Kit (Illumina) according to the manufacturer's instructions. This was sequenced
398 using a HiSeq 4000 with 2×151 bp reads. Raw FASTQ files were mapped to the *E. coli* W3110
399 genome sequence (NC_007779.1) using bwa (version 0.7.10) [49]; indel realignment and SNP
400 (single nucleotide polymorphism) calling was performed using Lofreq* (version 2.1.2) with
401 default parameters [50]. Resulting variants were assigned to associated genes and amino acid
402 changes using the Genbank Refseq W3110 annotation.
403
404 **Antibiotic sensitivity assay.** Sensitivity against different antibiotics was judged by efficiency of
405 plating (EOP) analyses on LB agar plates containing indicated concentrations of drugs. Briefly,
406 5-ml cultures were grown (inoculated with overnight cultures at 1:100 dilution) in LB broth at

407 37˚C until OD_{600} reached ~0.6. Cells were normalized according to OD_{600}, first diluted to OD_{600}
408 = 0.1 (~10^8 cells), and then serially diluted in LB with six 10-fold dilutions using 96-well
409 microtiter plates (Corning). Two microliters of the diluted cultures were manually spotted onto
410 the plates and incubated overnight at 37˚C.
411
412 **RNase I leakage assay.** Measurement of RNase I leakiness was performed using a plate assay as
413 described before [51]. Briefly, 5-ml cultures were grown (inoculated with overnight cultures at
414 1:100 dilution) in LB broth at 37˚C until OD_{600} reached ~0.6. Cells were normalized to OD_{600} =
415 0.001, and two microliters (~2,000 cells) were manually spotted onto LB agar plates containing
416 1.9 mg/ml yeast RNA extract (Sigma). The plates were incubated overnight at 37˚C. To
417 precipitate and visualize RNA, the plates were overlaid with cold (12.5% v/v) trichloroacetic
418 acid.
419
420 **Microscopy.** 5-ml cultures were grown (inoculated with overnight cultures at 1:100 dilution) in
421 LB broth at 37˚C until OD_{600} reached ~0.5 – 0.6. 5-µl cells were spotted onto freshly prepared 1%
422 agarose pads prepared in LB broth. Images were acquired using a FV1000 confocal microscope
423 (Olympus Fluoview FV1000, Tokyo, Japan) equipped with a 100x UPlanS Apo 1.4 NA oil
424 immersion objective and the Olympus Fluoview software. For each sample, the lengths and
425 widths of 100 cells were measured in Image J [52] and plotted using Graphpad prism 6.
426

427 **σ^E reporter assay.** Strains with plasmid expressing *rpoH*P3::*gfp* or promoterless *gfp* were grown
428 to mid-logarithmic phase (OD_{600} ≈ 0.4-0.6), then normalized and re-suspended in 150 mM NaCl.
429 Fluorescence level (Ex: 485 nm and Em: 535 nm) of equal amount of cells were measured for
430 each strain using the Victor X4 plate reader (Perkin Elmer). Relative levels of σ^E activation
431 correlates with the expression of GFP due to specific activation of *rpoH*P3 promoter and were
432 determined by normalizing the fluorescence level in strains with *rpoH*P3::*gfp* to the basal
433 fluorescence level in strains expressing *gfp* without promoter. Data from three independent
434 experiments were collected and normalized to the σ^E activation level in WT.
435
436 **Lipid extraction and liquid chromatography-mass spectrometry (LC-MS) analysis.** To
437 prepare the lipid extracts, a modified Bligh and Dyer method was used as described previously
438 [53]. Briefly, bacterial pellets were resuspended in PBS, and chloroform:methanol (1:2, v/v) was
439 added. The mixture was vortexed thoroughly before incubation with shaking at 1,000 rpm, 4°C.
440 Subsequently, water and chloroform were added to each sample to generate a two-phase
441 Bligh-Dyer mixture. The two phases were separated via centrifugation and the lower organic
442 phase was collected in a new tube. The aqueous phase was re-extracted twice with chloroform,
443 and all the organic extracts pooled and dried using a Centrivap and stored at -80°C until use.
444 The lipid samples were reconstituted in chloroform:methanol (1:1, v/v) and analyzed using a
445 high performance chromatography system (1260 Agilent Infinity Quaternary Pump) coupled to
446 an SCIEX QTOF 6600 mass spectrometer in negative electrospray ionization mode. Mass
447 calibration is performed every 5 h, using the automated calibration solution (SCIEX, Canada).

448 For lipid separation, normal phase chromatography was performed as previously described [53].
449 For characterization of the DAG-PP species using tandem mass spectrometry, multiple collision
450 energies ranging from -55 V to -85 V were used. MS and MS/MS spectra obtained were
451 visualized using Peak View (SCIEX) and graphical representations of the selected peaks of
452 interests were plotted using sigmaplot v10.0.
453
454 **OMV and membrane lipid composition analyses.** Steady-state [^{3}H]-glycerol-labelled PL
455 distributions in IMs/OMs, OMV levels, as well as PL/LPS ratios in [^{14}C]-acetate labelled
456 OMs/OMVs (see S7 Fig for workflow and raw data) were determined using methods previously
457 described [12].
458
459 **Phosphatidylglycerol (PG)/cardiolipin (CL) turnover assay.** Retrograde transport of OM
460 PG/CL can be inferred from turnover processes in the IM, which were monitored via [^{32}P]-pulse
461 chase experiments as previously described [12].
462
463 **SDS-PAGE and immunoblotting.** SDS-PAGE was performed according to Laemmli using the
464 12% or 15% Tris.HCl gels [54]. For ECA, cell samples were treated with proteinase K (0.25
465 mg/ml) at 55ºC for 1 h before loading and resolving on 10% Tricine SDS-PAGE gels.
466 Immunoblotting was performed by transferring from the gels onto polyvinylidene fluoride
467 (PVDF) membranes (Immun-Blot® 0.2 μm, Bio-Rad) using the semi-dry electroblotting system
468 (Trans-Blot® TurboTM Transfer System, Bio-Rad). Membranes were blocked using 1X casein

469 blocking buffer (Sigma). Rabbit α-LptE (from Daniel Kahne) was used at 1:5,000 dilutions.
470 Rabbit polyclonal α-ECA_{CYC} antisera (generous gift from Jolanta Lukasiewicz), which reacts
471 with all forms of ECA (ECA_{CYC}, ECA_{LPS}, ECA_{PG}), was used at 1:800 dilution [55]. Mouse
472 monoclonal α-LPS antibody (against LPS-core) was purchased from Hycult biotechnology and
473 used at 1:5,000 dilutions. α-mouse IgG secondary antibody conjugated to HRP (from sheep) and
474 α-rabbit IgG secondary antibody conjugated to HRP (from donkey) were purchased from GE
475 Healthcare and used at 1:5,000 dilutions. Luminata Forte Western HRP Substrate (Merck
476 Milipore) was used to develop the membranes and chemiluminescent signals were visualized by
477 G:BOX Chemi XT 4 (Genesys version1.3.4.0, Syngene).
478

Acknowledgements

X.E.J., R.S., and W.B.T. performed most of the experiments described in this work; S.L.C. analyzed the whole genome sequencing data of suppressor mutants; D.C.C.S. and X.L.G. performed the MS experiments; S.-S.C. directed and supervised the work; X.E.J., R.S., W.B.T., and S.-S.C. analyzed the data and wrote the paper; all authors provided critical feedback of the manuscript. We thank Majid Eshaghi (Genome Institute of Singapore, GIS) for providing σ^E reporter plasmids and Kevin Young (University of Arkansas for Medical Sciences) for the generous gifts of the Δ*wcaJ* strain and the *uppS* overexpression plasmid. We are grateful to Jolanta Łukasiewicz (Polish Academy of Sciences) and Daniel Kahne (Harvard University) for the α-ECA and α-LptE antibodies, respectively. We also thank William F. Burkholder (CZ Biohub) for useful discussions. WGS work was partially supported by the GIS, and the Singapore Ministry of Health National Medical Research Council (NMRC/CIRG/1357/2013) to S.L.C.. Lipid MS analysis was supported by the Nanyang Assistant Professorship to X.L.G.. All other work were supported by the National University of Singapore Start-up funding, the Singapore Ministry of Education Academic Research Fund Tier 1 Grant, and the Singapore Ministry of Health National Medical Research Council under its Cooperative Basic Research Grant (NMRC/CBRG/0072/2014) to S.-S.C.. The authors declare no conflict of interest.

497 **References**

498

499 1. Nikaido H. Molecular basis of bacterial outer membrane permeability revisited. Microbiol Mol
500 Biol Rev. 2003;67: 593–656.
501 2. Raetz CR, Whitfield C. Lipopolysaccharide endotoxins. Annu Rev Biochem. 2002;71:
502 635–700.
503 3. Okuda S, Sherman DJ, Silhavy TJ, Ruiz N, Kahne D. Lipopolysaccharide transport and
504 assembly at the outer membrane: the PEZ model. Nat Rev Microbiol. 2016;14: 337–345.
505 4. Hagan CL, Silhavy TJ, Kahne D. β-barrel membrane protein assembly by the Bam complex.
506 Annu Rev Biochem. 2011;80: 189–210.
507 5. Okuda S, Tokuda H. Lipoprotein sorting in bacteria. Annu Rev Microbiol. 2011;65: 239–259.
508 6. Donohue-Rolfe AM, Schaechter M. Translocation of phospholipids from the inner to the outer
509 membrane of *Escherichia coli*. Proc Natl Acad Sci USA. 1980;77: 1867–1871.
510 7. Jones NC, Osborn MJ. Translocation of phospholipids between the outer and inner membranes
511 of *Salmonella typhimurium*. J Biol Chem. 1977;252: 7405–7412.
512 8. Langley KE, Hawrot E, Kennedy EP. Membrane assembly: movement of phosphatidylserine
513 between the cytoplasmic and outer membranes of *Escherichia coli*. J Bacteriol. 1982;152:
514 1033–1041.
515 9. Grabowicz M, Silhavy TJ. Envelope stress responses: an interconnected safety net. Trends Cell
516 Biol. 2017;42: 232–242.

517 10. Raivio TL. Everything old is new again: an update on current research on the Cpx envelope
518 stress response. Biochim Biophys Acta. 2014;1843: 1529–1541.
519 11. Majdalani N, Gottesman S. The Rcs phosphorelay: a complex signal transduction system.
520 Annu Rev Microbiol. 2005;59: 379–405.
521 12. Shrivastava R, Xiang'Er J, Chng SS. Outer membrane lipid homeostasis via retrograde
522 phospholipid transport in *Escherichia coli*. Mol Microbiol. 2017;106: 395–408.
523 13. Lloubes R, Cascales E, Walburger A, Bouveret E, Lazdunski C, Bernadac A, Journet L. The
524 Tol-Pal proteins of the *Escherichia coli* cell envelope: an energized system required for outer
525 membrane integrity? Res Microbiol. 2001;152: 523–529.
526 14. Sturgis JN. Organisation and evolution of the *tol-pal* gene cluster. J Mol Microbiol
527 Biotechnol. 2001;3: 113–122.
528 15. Cascales E, Gavioli M, Sturgis JN, Lloubes R. Proton motive force drives the interaction of
529 the inner membrane TolA and outer membrane Pal proteins in *Escherichia coli*. Mol
530 Microbiol. 2000;38: 904–915.
531 16. Bernadac A, Gavioli M, Lazzaroni JC, Raina S, Lloubes R. *Escherichia coli tol-pal* mutants
532 form outer membrane vesicles. J Bacteriol. 1998;180: 4872–4878.
533 17. Gerding MA, Ogata Y, Pecora ND, Niki H, de Boer PAJ. The trans-envelope Tol-Pal
534 complex is part of the cell division machinery and required for proper outer-membrane
535 invagination during cell constriction in *E. coli*. Mol Microbiol. 2007;63: 1008–1025.
536 18. Kuhn H, Meier-Dieter U, Mayer H. ECA, the enterobacterial common antigen. FEMS
537 Microbiol Lett. 1988;54: 195–222.

538 19. Krishnamoorthy G, Wolloscheck D, Weeks JW, Croft C, Rybenkov VV, Zgurskaya HI.
539 Breaking the permeability barrier of *Escherichia coli* by controlled hyperporination of the
540 outer membrane. Antimicrob Agents Chemother. 2016;60: 7372–7381.
541 20. Meier-Dieter U, Starman R, Barr K, Mayer H, Rick PD. Biosynthesis of enterobacterial
542 common antigen in *Escherichia coli*. Biochemical characterization of *Tn10* insertion mutants
543 defective in enterobacterial common antigen synthesis. J Biol Chem. 1990;265: 13490–13497.
544 21. Khetrapal V, Mehershahi K, Rafee S, Chen S, Lim CL, Chen SL. A set of powerful negative
545 selection systems for unmodified Enterobacteriaceae. Nucleic Acids Res. 2015;43: e83.
546 22. Castelli ME, Véscovi EG. The Rcs signal transduction pathway is triggered by enterobacterial
547 common antigen structure alterations in *Serratia marcescens*. J Bacteriol. 2011;193: 63–74.
548 23. Clavel T, Lazzaroni JC, Vianney A, Portalier R. Expression of the *tolQRA* genes of
549 *Escherichia coli* K-12 is controlled by the RcsC sensor protein involved in capsule synthesis.
550 Mol Microbiol. 1996;19: 19–25.
551 24. Stout V, Gottesman S. RcsB and RcsC: a two-component regulator of capsule synthesis in
552 *Escherichia coli*. J Bacteriol. 1990;172: 659–669.
553 25. Trisler P, Gottesman S. lon transcriptional regulation of genes necessary for capsular
554 polysaccharide synthesis in *Escherichia coli* K-12. J Bacteriol. 1984;160: 184–191.
555 26. Stevenson G, Andrianopoulos K, Hobbs M, Reeves PR. Organization of the *Escherichia coli*
556 K-12 gene cluster responsible for production of the extracellular polysaccharide colanic acid. J
557 Bacteriol. 1996;178: 4885–4893.

558 27. Rahman A, Barr K, Rick PD. Identification of the structural gene for the TDP-Fuc4NAc:lipid
559 II Fuc4NAc transferase involved in synthesis of enterobacterial common antigen in *Escherichia*
560 *coli* K-12. J Bacteriol. 2001;183: 6509–6516.
561 28. Rick PD, Barr K, Sankaran K, Kajimura J, Rush JS, Waechter CJ. Evidence that the *wzxE* gene
562 of *Escherichia coli* K-12 encodes a protein involved in the transbilayer movement of a
563 trisaccharide-lipid intermediate in the assembly of enterobacterial common antigen. J Biol
564 Chem. 2003;278: 16534–16542.
565 29. Kajimura J, Rahman A, Rick PD. Assembly of cyclic enterobacterial common antigen in
566 *Escherichia coli* K-12. J Bacteriol. 2005;187: 6917–6927.
567 30. Barr K, Klena J, Rick PD. The modality of enterobacterial common antigen polysaccharide
568 chain lengths is regulated by o349 of the *wec* gene cluster of *Escherichia coli* K-12. J Bacteriol.
569 1999;181: 6564–6568.
570 31. Kuhn HM, Neter E, Mayer H. Modification of the lipid moiety of the enterobacterial common
571 antigen by the "Pseudomonas factor". Infect Immun. 1983;40: 696–700.
572 32. Rinno J, Golecki JR, Mayer H. Localization of enterobacterial common antigen: immunogenic
573 and nonimmunogenic enterobacterial common antigen-containing *Escherichia coli*. J Bacteriol.
574 1980;141: 814–821.
575 33. Acker G, Bitter-Suermann D, Meier-Dieter U, Peters H, Mayer H. Immunocytochemical
576 localization of enterobacterial common antigen in *Escherichia coli* and *Yersinia enterocolitica*
577 cells. J Bacteriol. 1986;168: 348–356.

578 34. Meier-Dieter U, Barr K, Starman R, Hatch L, Rick PD. Nucleotide sequence of the *Escherichia*
579 *coli rfe* gene involved in the synthesis of enterobacterial common antigen. Molecular cloning of
580 the *rfe-rff* gene cluster. J Biol Chem. 1992;267: 746–753.
581 35. Baba T, Ara T, Hasegawa M, Takai Y, Okumura Y, Baba M, Datsenko KA, Tomita M, Wanner
582 BL, Mori H. Construction of *Escherichia coli* K-12 in-frame, single-gene knockout mutants:
583 the Keio collection. Mol Syst Biol. 2006;2: 2006.0008.
584 36. MacCain WJ, Kannan S, Jameel DZ, Troutman JM, Young KD. A defective undecaprenyl
585 pyrophosphate synthase induces growth and morphological defects that are suppressed by
586 mutations in the isoprenoid pathway of *Escherichia coli*. J Bacteriol. 2018;200: e00255-18.
587 37. Jorgenson MA, Kannan S, Laubacher ME, Young KD. Dead-end intermediates in the
588 enterobacterial common antigen pathway induce morphological defects in *Escherichia coli* by
589 competing for undecaprenyl phosphate. Mol Microbiol. 2016;100: 1–14.
590 38. Danese PN, Oliver GR, Barr K, Bowman GD, Rick PD, Silhavy TJ. Accumulation of the
591 enterobacterial common antigen lipid II biosynthetic intermediate stimulates *degP* transcription
592 in *Escherichia coli*. J Bacteriol. 1998;180: 5875–5884.
593 39. Rick PD, Hubbard GL, Kitaoka M, Nagaki H, Kinoshita T, Dowd S, Simplaceanu V, Ho C.
594 Characterization of the lipid-carrier involved in the synthesis of enterobacterial common
595 antigen (ECA) and identification of a novel phosphoglyceride in a mutant of *Salmonella*
596 *typhimurium* defective in ECA synthesis. Glycobiology. 1998;8: 557–567.
597 40. Oursel D, Loutelier-Bourhis C, Orange N, Chevalier S, Norris V, Lange CM. Lipid
598 composition of membranes of *Escherichia coli* by liquid chromatography/tandem mass

599 spectrometry using negative electrospray ionization. Rapid Commun Mass Spectrom. 2018;21:
600 1721–1728.
601 41. McMahon KJ, Castelli ME, Garcia Vescovi E, Feldman MF. Biogenesis of outer membrane
602 vesicles in *Serratia marcescens* is thermoregulated and can be induced by activation of the Rcs
603 phosphorelay system. J Bacteriol. 2012;194: 3241–3249.
604 42. Masilamani R, Cian MB, Dalebroux ZD. *Salmonella* Tol-Pal reduces outer membrane
605 glycerophospholipid levels for envelope homeostasis and survival during bacteremia. Infect
606 Immun. 2018;86: e00173–18.
607 43. Mitchell AM, Srikumar T, Silhavy TJ. Cyclic enterobacterial common antigen maintains the
608 outer membrane permeability barrier of *Escherichia coli* in a manner controlled by YhdP.
609 MBio. 2018;9: e01321–18.
610 44. Jorgenson MA, Young KD. Interrupting biosynthesis of O antigen or the lipopolysaccharide
611 core produces morphological defects in *Escherichia coli* by sequestering undecaprenyl
612 phosphate. J Bacteriol. 2016;198: 3070–3079.
613 45. Casadaban MJ. Transposition and fusion of the *lac* genes to selected promoters
614 in *Escherichia coli* using bacteriophage lambda and Mu. J Mol Biol. 1976;104: 541–555.
615 46. Ruiz N, Gronenberg LS, Kahne D, Silhavy TJ. Identification of two inner-membrane proteins
616 required for the transport of lipopolysaccharide to the outer membrane of *Escherichia coli*.
617 Proc Natl Acad Sci USA. 2008;105: 5537–5542.
618 47. Datsenko KA, Wanner BL. One-step inactivation of chromosomal genes in *Escherichia coli*
619 K-12 using PCR products. Proc Natl Acad Sci USA. 2008;97: 6640–6645.

620 48. Silhavy TJ, Berman ML, Enquist LW. Experiments with Gene fusions. New York: Cold
621 Spring Harbor Laboratory; 1984.
622 49. Li H, Durbin R. Fast and accurate short read alignment with Burrows-Wheeler Transform.
623 Bioinformatics. 2009;25: 1754–60.
624 50. Wilm A, Aw PP, Bertland D, Yeo GH, Ong SH, Wong CH, Khor CC, Petric R, Hibberd ML,
625 Nagarajan N. LoFreq: a sequence-quality aware, ultra-sensitive variant caller for uncovering
626 cell-population heterogeneity from high-throughput sequencing datasets. Nucleic Acids Res.
627 2012;40: 11189–11201.
628 51. Lazzaroni JC, Portalier RC. Isolation and preliminary characterization of periplasmic-leaky
629 mutants of *Escherichia coli* K-12. FEMS Microbiol Lett. 1979;5: 411–416.
630 52. Schneider CA, Rasband WS, Eliceiri KW. NIH image to ImageJ: 25 years of image analysis.
631 Nat methods. 2012;9: 671–675.
632 53. Guan XL, Mäser P. Comparative sphingolipidomics of disease-causing trypanosomatids rveal
633 unique lifecycle- and taxonomy-specific lipid chemistries. Sci Rep. 2017;7: 13617.
634 54. Laemmli UK. Cleavage of structural proteins during the assembly of the head of
635 bacteriophage T4. Nature. 1970;227: 680–685.
636 55. Gozdzlewicz TK, Lugowski C, Lukasiewicz J. First evidence for a covalent linkage between
637 enterobacterial common antigen and lipopolysaccharide in *Shigella sonnei* phase II ECALPS.
638 J Biol Chem. 2014;289: 2745–2754.
639 56. Hawrot E, Kennedy EP. Phospholipid composition and membrane function in
640 phosphatidylserine decarboxylase mutants of *Escherichia coli*. J Biol Chem. 1978;253:

641 8213–8220.

642 57. Raivio TL, Popkin DL, Silhavy TJ. The Cpx envelope stress response is controlled by
643 amplification and feedback inhibition. J Bacteriol. 1999;181: 5263–5272.

644 58. Cherepanov PP, Wackernagel W. Gene disruption in *Escherichia coli*: TcR and KmR
645 cassettes with the option of Flp catalyzed excision of the antibiotic-resistance determinant.
646 Gene. 1995;158: 9–14.

647 59. Pitre A, Pan Y, Pruett S, Skalli O. On the use of ratio standard curves to accurately quantitate
648 relative changes in protein levels by western blot. Anal Biochem. 2007;361: 305–307.

649 60. Yokoto K, Kito M. Transfer of the phosphatidyl moiety of phosphatidylglycerol to
650 phosphatidylethanolamine in *Escherichia coli*. J Bacteriol. 1982;151: 952–961.

651 61. Audet A, Cole R, Proulx P. Polyglycerophosphatide metabolism in *Escherichia coli*. Biochim
652 Biophys Acta. 1975;380: 414–420.

Figure legends

Fig 1 Loss-of-function mutations in the ECA pathway rescue vancomycin sensitivity in *tol-pal* mutants. Vancomycin sensitivity of indicated *tol-pal* strains with or without (A) *wecC**, (B) Δ*wecC*, and (D) Δ*wecB*/Δ*wecF* mutations based on efficiency of plating (EOP) on LB agar plates supplemented with vancomycin (120 μg/ml). (C) ECA levels in WT and Δ*tolA* strains with or without *wecC** and Δ*wecC* mutations as judged by immunoblot analysis using α-ECA antibody. Samples were normalized by OD_{600} and treated with proteinase K prior to Tricine SDS-PAGE/immunoblotting.

Fig 2 Restoration of OM permeability defects by Δ*wecC* in cells lacking TolA does not require the Rcs phosphorelay cascade and/or capsular polysaccharide biosynthesis. (A) Vancomycin sensitivity of indicated strains in either Δ*rcsC* or Δ*wcaJ* backgrounds based on EOP on LB agar plates supplemented with vancomycin (120 μg/ml). (B) RNase I leakage in the same strains as (A), as judged by RNA degradation (halo formation) around cells spotted on LB agar plates containing yeast RNA, subsequently precipitated with trichloroacetic acid.

Fig 3 Accumulation of ECA biosynthetic intermediates restores vancomycin resistance in cells lacking TolA. (A) Schematic of the ECA biosynthetic pathway illustrating und-PP-GlcNAc-ManNAcA-Fuc4NAc (Lipid III^{ECA}) synthesis at the inner leaflet of IM, and subsequent polymerization at the outer leaflet. The final ECA polymer (ECA_{PG}) is attached to a

674 phosphoglyceride (i.e. diacylglycerol-phosphate (DAG-P) aka phosphatidic acid) and transported
675 to the OM. Chemical structures of und-PP and DAG-P anchors are shown. (B, C) Vancomycin
676 sensitivity of the Δ*wcaJ* Δ*tolA* strain with or without indicated *wec* mutations in otherwise (B)
677 WT or (C) Δ*wecA* backgrounds, based on efficiency of plating (EOP) on LB agar plates
678 supplemented with vancomycin (120 ug/ml).
679
680 **Fig 4** Partial accumulation of Lipid III^{ECA} and/or short chain ECA rescues vancomycin
681 sensitivity in cells lacking TolA. (A) Vancomycin sensitivity of the Δ*wcaJ* Δ*tolA* strain with or
682 without Δ*wzzE* mutation in otherwise WT or Δ*wecA* backgrounds, based on efficiency of plating
683 (EOP) on LB agar plates supplemented with vancomycin (120 ug/ml). (B) ECA profiles in the
684 indicated Δ*wcaJ* strains as judged by immunoblot analysis using α-ECA antibody. Samples were
685 normalized by OD_{600} and treated with proteinase K prior to Tricine SDS-PAGE/immunoblotting.
686 Profiles in strains progressively depleted of *wzyE* are used to visualize accumulation of Lipid
687 III^{ECA}. Relative band intensities from ECA profiles of WT, Δ*wzzE,* and *wzyE*-depleted (*) strains
688 are shown on the right.
689
690 **Fig 5** Strains lacking WecG or WecC accumulate DAG-PP-GlcNAc species in the IM. (A) Ion
691 chromatogram (XIC) of 34:1 DAG-PP-GlcNAc (m/z 956.5243) extracted from LC-MS analyses
692 of total lipids isolated from indicated Δ*wcaJ* strains. Inset, XICs of corresponding 32:1 (m/z
693 928.4927), 34:2 (954.5076) and 36:1 (m/z 982.5391) species. (B) Mass spectra obtained from
694 integration of XIC peak region in (A) of Δ*wcaJ* (WT) and Δ*wcaJ* Δ*wecG* strains. WT peaks

(black) are overlaid on top of Δ*wecG* peaks (red), illustrating unique DAG-PP-GlcNAc signals in the latter strain. (C) XICs of 34:1 DAG-PP-GlcNAc (m/z 956.5243) extracted from LC-MS analyses of IM lipids isolated from indicated Δ*wcaJ* strains. Inset, XICs of the same species from OM lipids.

Fig 6 The chemical structures of DAG-PP-GlcNAc species are deduced from MS fragmentation analysis. (A) Proposed fragmentation pattern with mass assignments of 32:1 and 34:1 DAG-PP-GlcNAc species. (B and C) MS/MS spectra of (B) 32:1 and (C) 34:1 DAG-PP-GlcNAc species at indicated collision energies. Spectrum at high collision energy (-75 V, red) is overlaid on top of that at low collision energy (-55 V, black).

Fig 7 Accumulation of ECA intermediates restores OM lipid homeostasis in cells lacking TolA. (A) *left*, Representative [^{3}H]-distribution profiles of cell lysates from indicated Δ*wcaJ* strains, fractionated on sucrose density gradients. Cells were grown in the presence of [2-^{3}H]glycerol to specifically label PLs in the IMs and OMs. Total [^{3}H]-activities detected in IM (6–10) and OM (12–14) fractions were expressed as a percentage of their sums, averaged across three replicate experiments. *right*, Steady-state distribution of [^{3}H]-glycerol labelled PLs between the IM and the OM of indicated Δ*wcaJ* strains (*left panel*). Distribution of [^{3}H]-labelled PLs in the OMs of respective mutants expressed as fold changes relative to the WT OM (*right panel*). (B) Steady-state PL:LPS ([^{14}C]-acetate labelled) ratios in the OMs and OMVs of indicated Δ*wcaJ* strains (*left panel*). OM PL:LPS ratios of respective mutants, and OMV PL:LPS ratios of Δ*tolA*

716 and Δ*tolA* Δ*wecC* mutant strains, expressed as fold changes relative to that in the WT OM (*right*
717 *panel*). Error bars represent standard deviations calculated from triplicate experiments. Student's
718 t-tests: * $p < 0.05$ (as compared to WT).

719

720 **Supporting information legend**

721

722 **S1 Appendix** (includes S1-S10 Fig, S1-S4 Table)

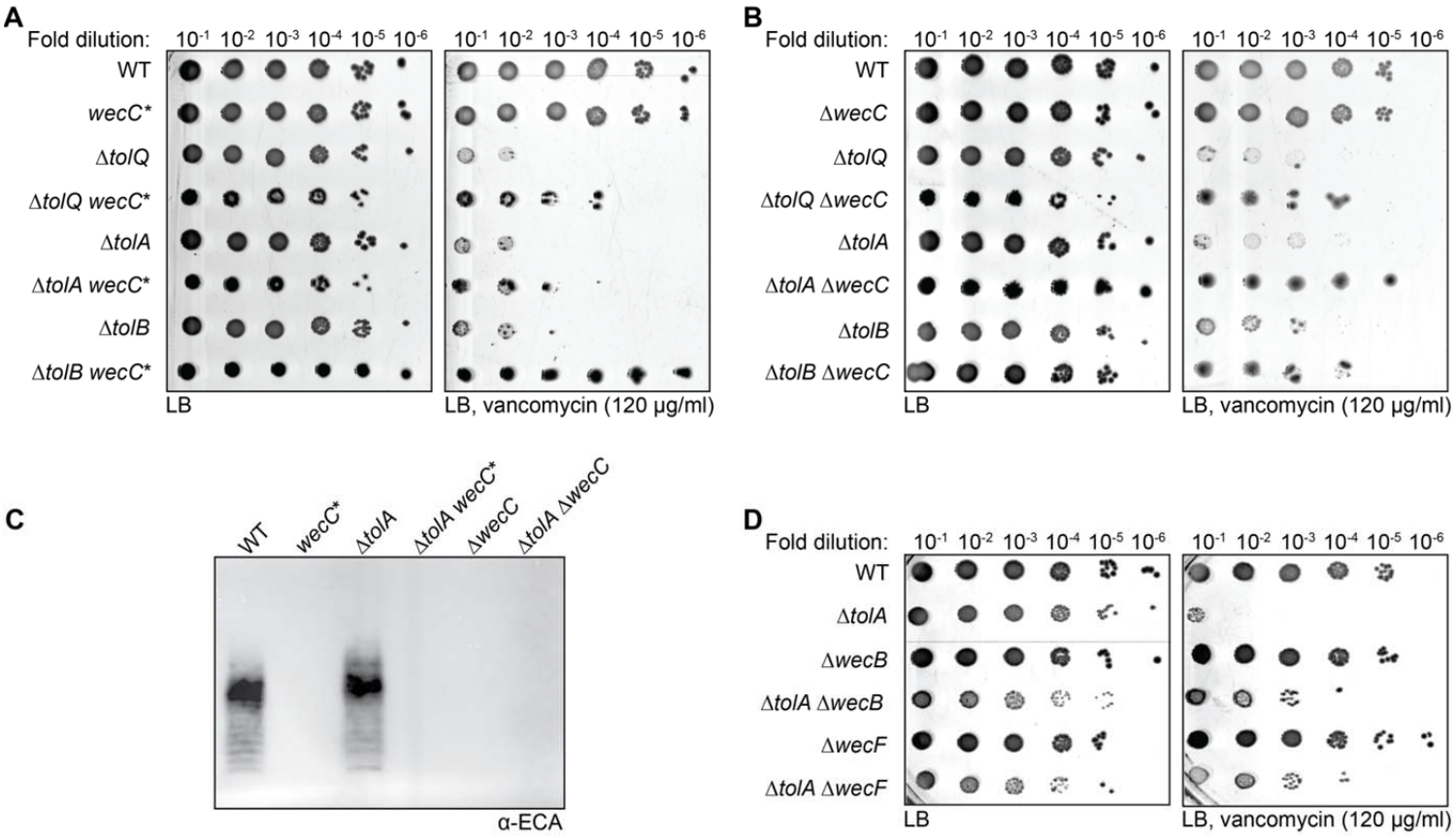

Fig 1

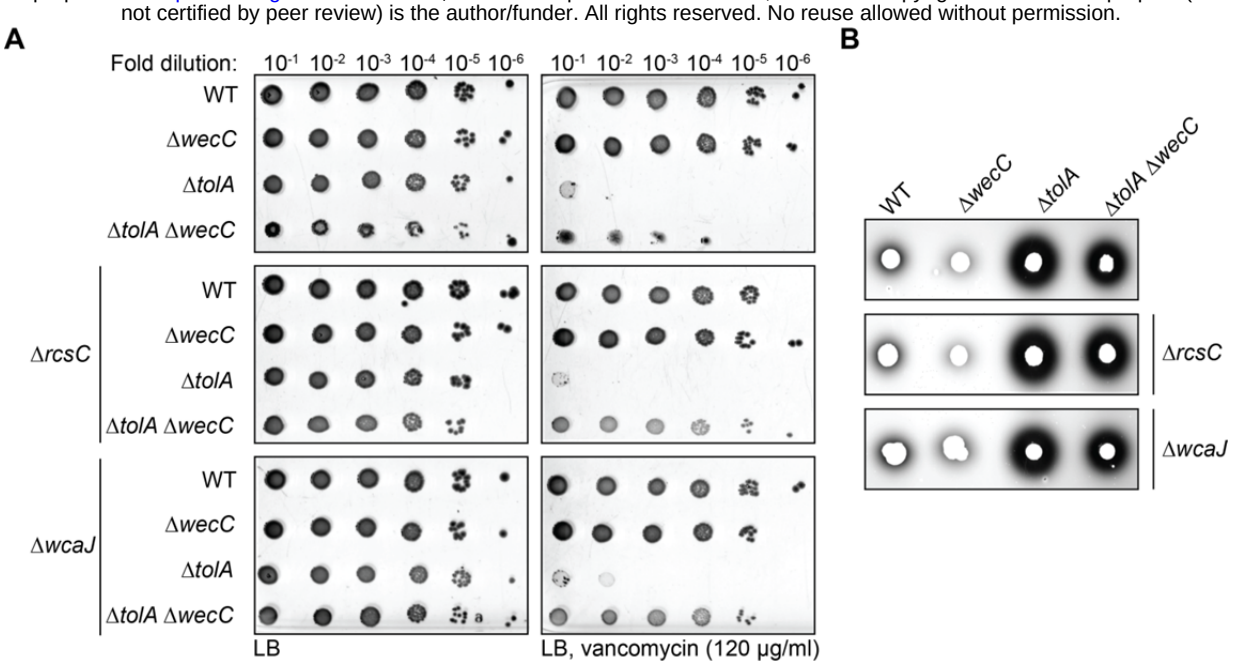

Fig 2

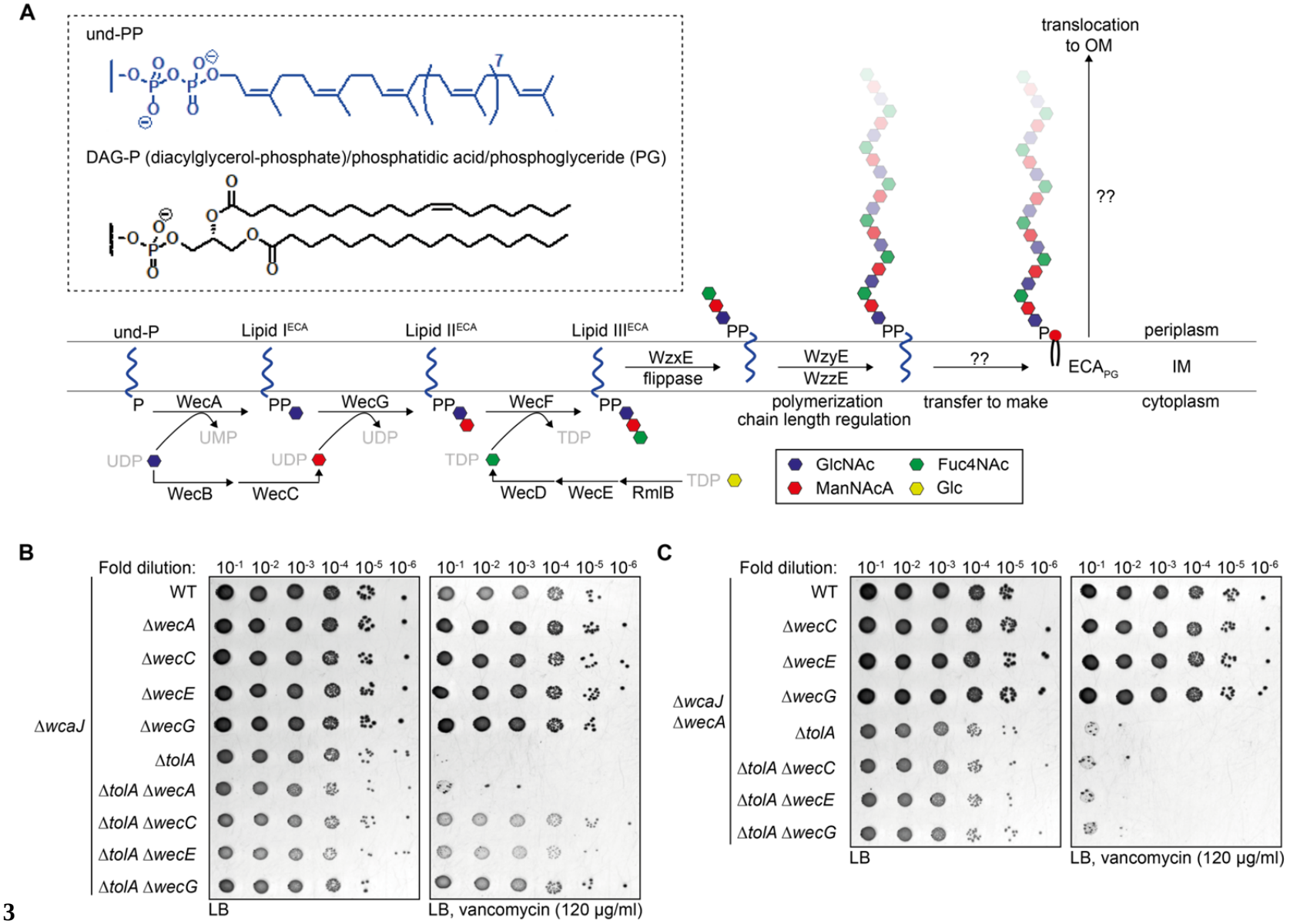

Fig 3

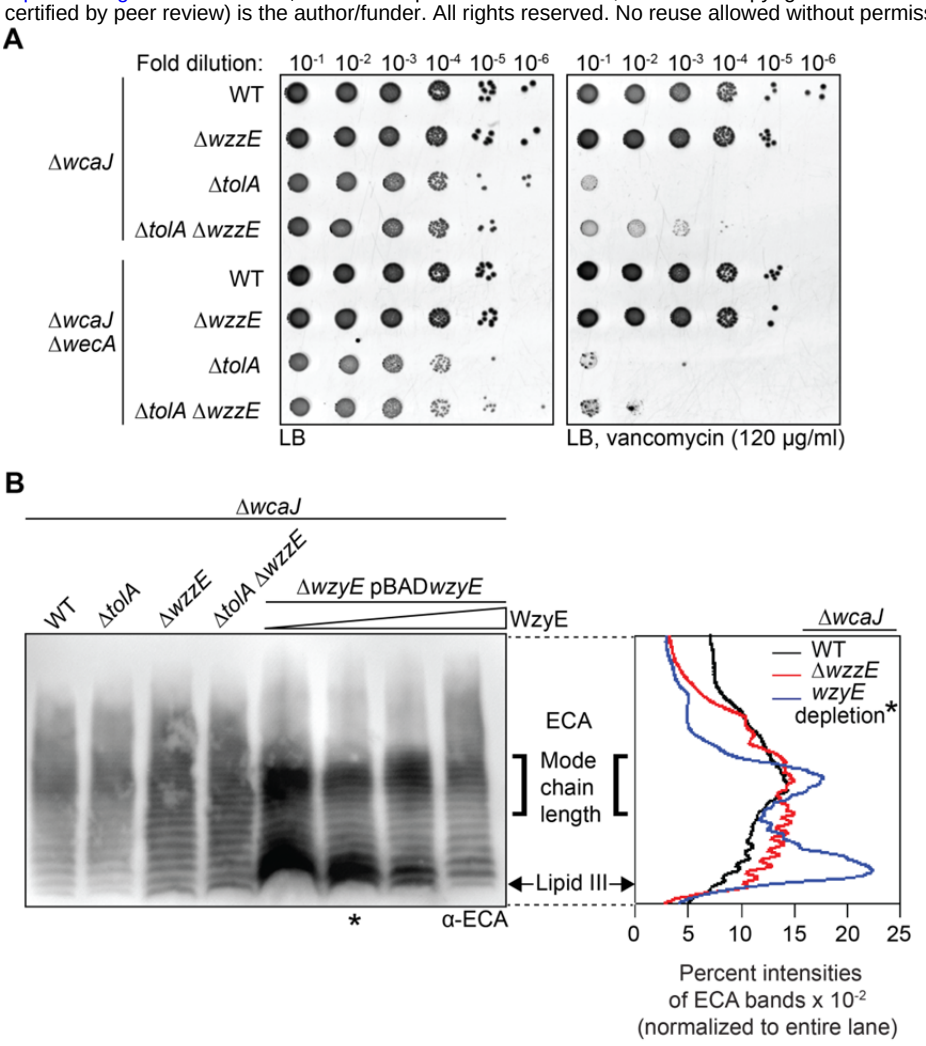

Fig 4

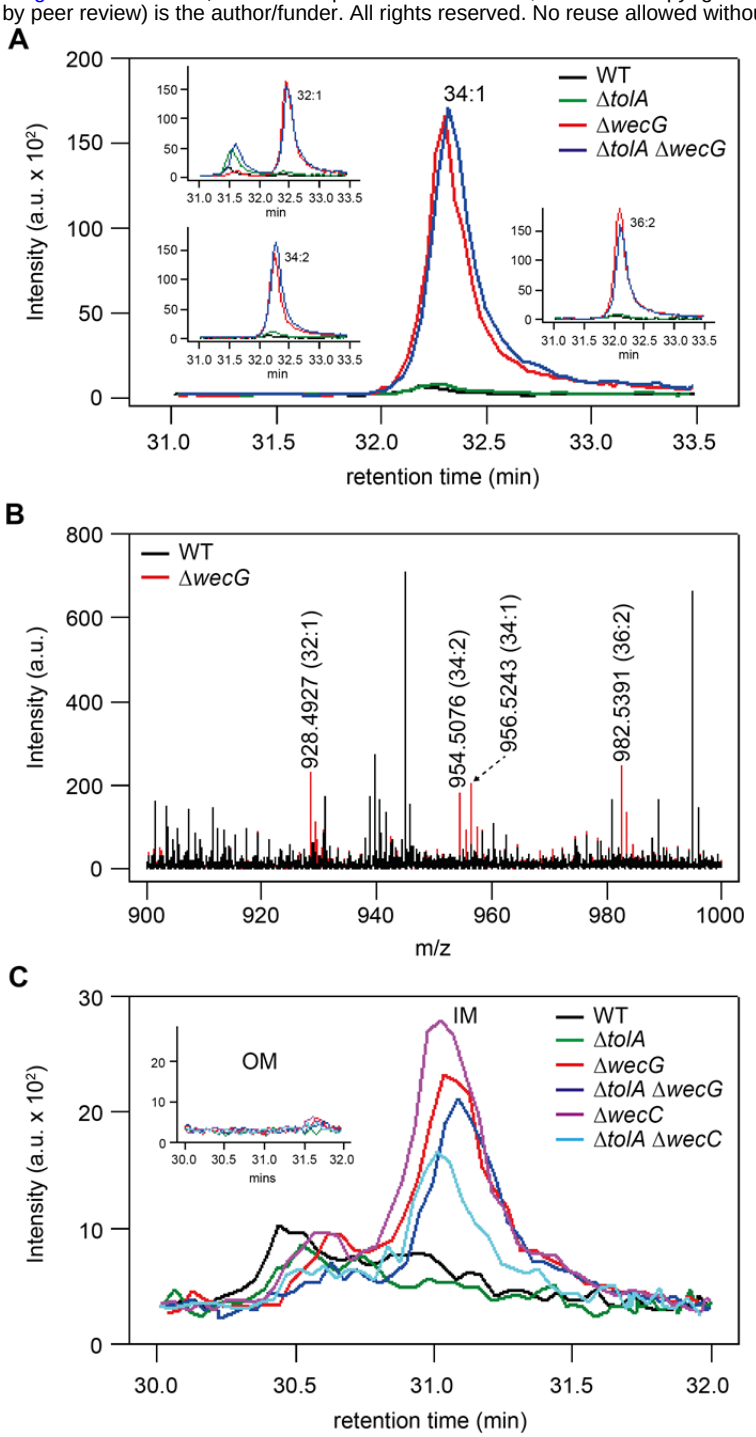

Fig 5

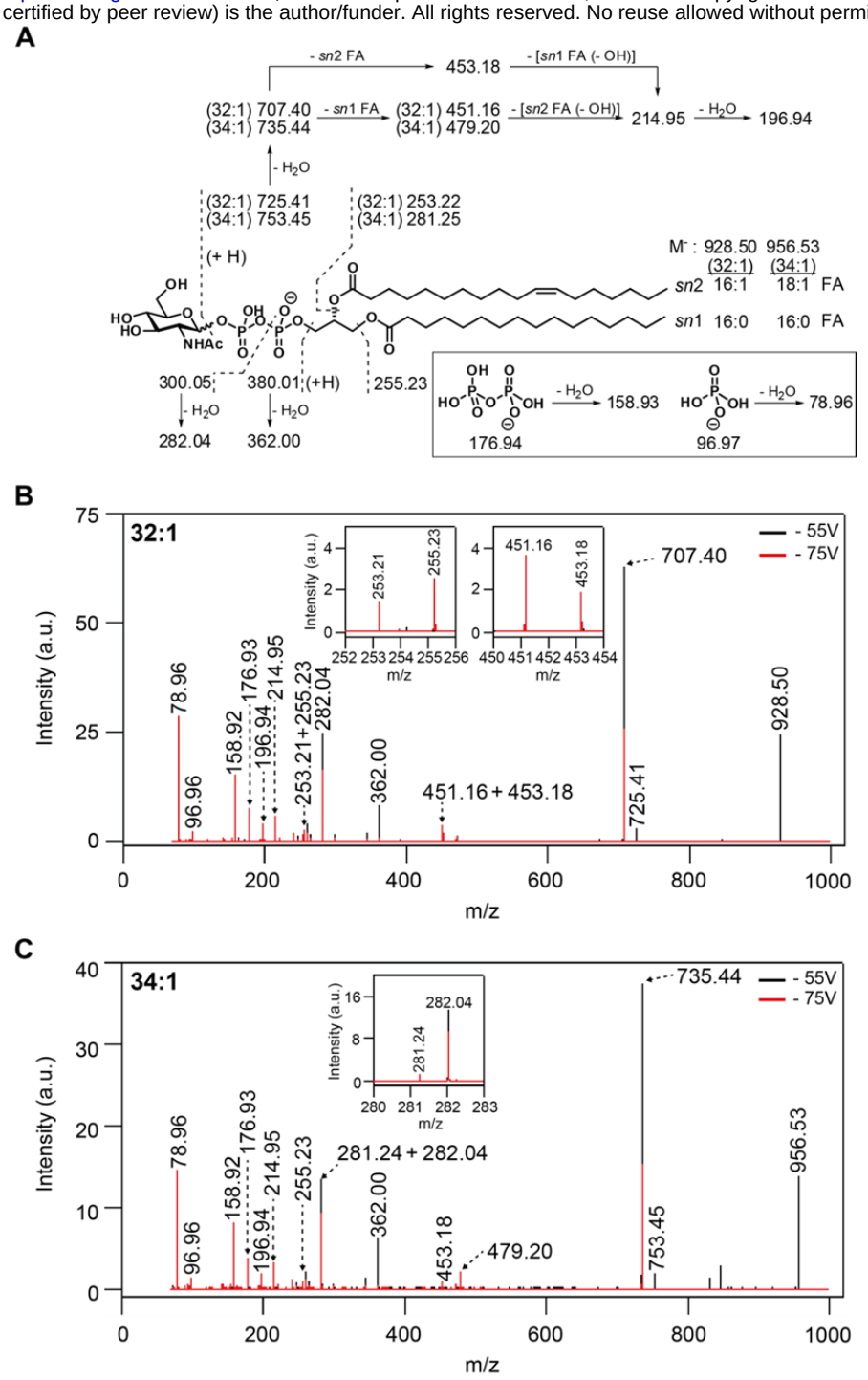

Fig 6

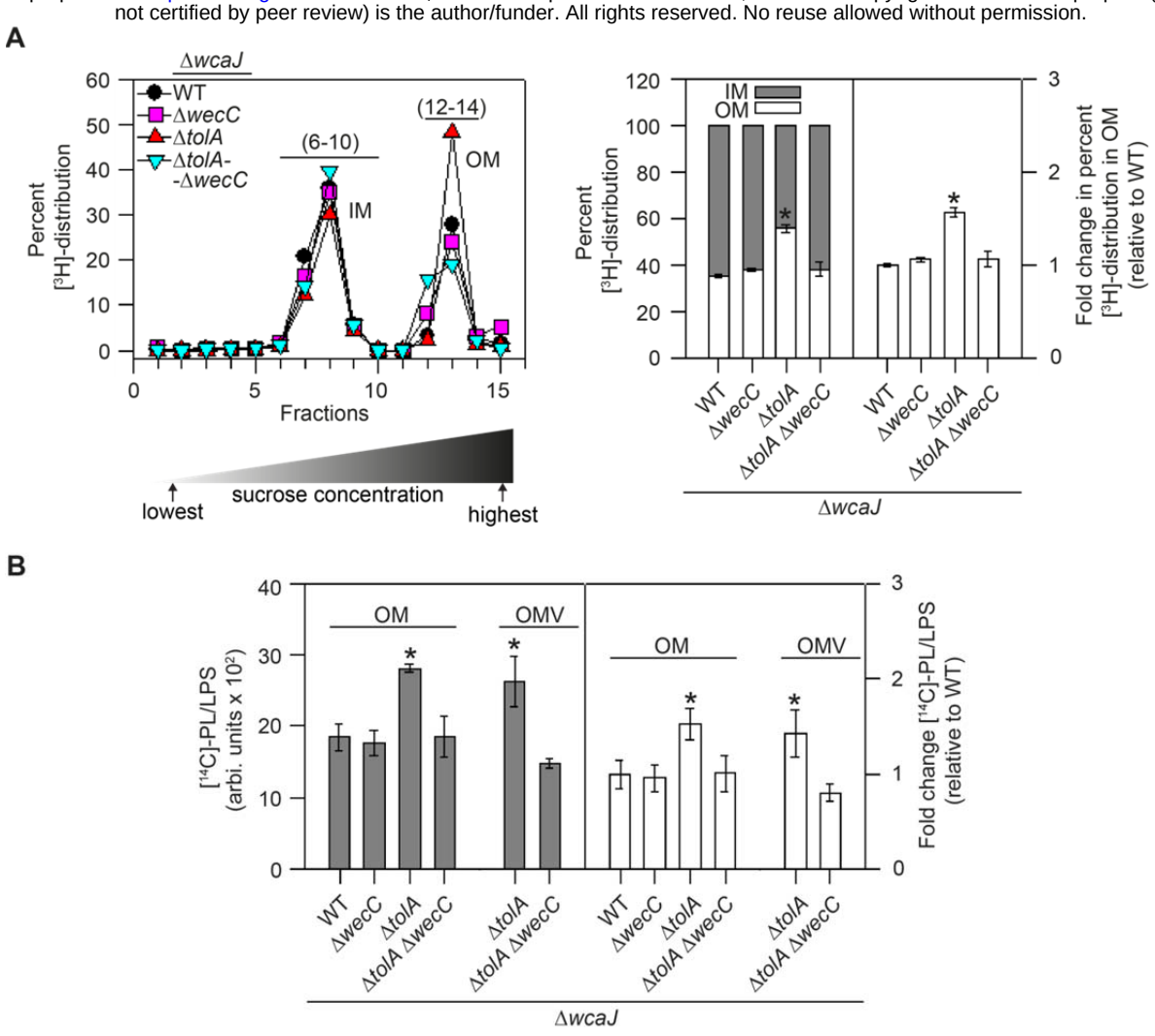

Fig 7